Book of Tutorials and Abstracts

European Microbeam Analysis Society

EMAS 2019

16th

EUROPEAN WORKSHOP

on

MODERN DEVELOPMENTS AND APPLICATIONS IN MICROBEAM ANALYSIS

19 to 23 May 2019
at the
NTNU, Realfagbygget
Trondheim, Norway

Organised in collaboration with:
Norwegian University of Science and Technology
(NTNU)

A MULTI-PLATFORM APPROACH TO ORE MINERALOGY: ADVANCES AND FUTURE PROSPECTS

Angus K.O. Netting[1,*], C.L. Ciobanu[2], N.J. Cook[2], B.P. Wade[1], A. Slattery[1], M.R. Verdugo-Ihl[2], L. Courtney-Davies[2] and K. Ehrig[3]

1 The University of Adelaide, Adelaide Microscopy
Frome Road, 5005 Adelaide, SA, Australia
2 The University of Adelaide, School of Chemical Engineering
5000 Adelaide, SA, Australia
3 BHP Olympic Dam
5000 Adelaide, SA, Australia.
e-mail: angus.netting@adelaide.edu.au

Angus Netting currently holds the position of Director of Adelaide Microscopy and Adelaide Biobank, the University of Adelaide's centre for Advanced Microscopy and Microanalysis. Angus studied Physical Chemistry at Flinders University, South Australia, in the early 1980's and worked as an industrial chemist for a number of years before taking up a position in Surface Analysis (XPS and Scanning Auger Microscopy) at the University of South Australia.

He later became manager of scientific consulting services at the Ian Wark Research Institute before joining the University of Adelaide in 2001 as a Senior Microscopist in EPMA and analytical SEM. He was appointed deputy director of Adelaide Microscopy in 2009 and Director in 2014. His main area of interest is in X-ray microanalysis techniques in electron microscopy. He has held the position of Secretary of AMAS from 2002-2009, President of the Microbeam Analysis Society of Australia (AMAS) from 2010-2012, and has commenced a second term as AMAS President in 2019. Angus is currently the South Australian Node Director for Microscopy Australia. He convened the 10th AMAS Symposium in Adelaide in 2009 and the 23rd Australian Conference for Microscopy and Microanalysis in 2014.

1. ABSTRACT

In the last decade, the rapid technological advancement of micro- and nanoimaging and microanalysis techniques has transformed the field of ore mineralogy. The improved spatial resolution and limit of detection of these techniques has allowed the physical and chemical signature of the minerals to be determined that would otherwise have been impossible in the not too distant past. The technological advancement of these techniques has met with a concurrent change to the way we approach analytical mineralogy. Increases in the sensitivity of analytical instruments now allows critical petrogenetic trace chemical data to be obtained from minerals that were otherwise impossible to analyse quantitatively with microbeam techniques. In situ nanoscale imaging and analytical characterisation is becoming an increasingly important field for understanding how the chemical signatures we measure at the micrometre-scale are distributed at the atomic level within the mineral. A complementary and crucial aspect of these imaging and analytical techniques has been the development of new geochronometers such as the U-Pb hematite geochronometer, allowing for important temporal information to be assigned to observable chemical changes. As a result, there is an increasing recognition that a holistic approach, encompassing both ore minerals and gangue, and across all spatial scales, is necessary. In the context of the ore deposit that hosts them, the chemical and structural characterisation of mineral assemblages can give important insights on fundamental questions of solid-state chemistry and ore-forming processes. It follows that broad regional- or deposit-scale genetic models can be tested and validated via observation and analysis of minerals down to the smallest scale, thus enabling improved exploration models. Increased volumes of data generated at different scales of observation on the same samples will in turn generate additional fundamental questions and catalyse further technological advancements. Fields likely to be the focus of future advancement include the atomic-scale distribution of metals within ore minerals, and the roles played by nanoparticles in that distribution. This includes observation of lattice-scale structural changes to minerals as they incorporate these metals as a response to changing physiochemical conditions.

2. INTRODUCTION

The present-day ore mineralogist is tremendously fortunate to have a large number of advanced analytical methods at hand, which can, particularly when used in combination, in-situ, on the same material, and bridging different scales of observation, provide extraordinary levels of information impossible a generation ago [1]. Although the generation of large volumes of data can at times present its own problems regarding the necessity of rigorous, time-consuming data quality control, and increased resolution of ever smaller features may often expose unexplained complexities, it is nevertheless an extraordinarily exciting time to be working in the field.

Using examples from published work carried out in the laboratories of Adelaide Microscopy, we show how increased analytical capabilities offer the potential to resolve outstanding questions in

ore mineralogy. Analytical techniques and methodologies reviewed here include laser ablation inductively coupled plasma mass spectrometry (LA-ICP-MS); recent developments in U-Pb hematite geochronology and associated preparation of a matrix-matched hematite standard for microbeam analysis; and high-angle annular dark field scanning transmission electron microscopy (HAADF STEM) applied to mixed-layer minerals, nanoparticle mapping and other problems in ore mineralogy.

3. LA-ICP-MS; IMAGING OF TRACE ELEMENTS AND TEMPORAL CONSTRAINTS

The ability to both accurately and precisely measure trace chemical variations of minerals in-situ has led to a prolific increase of this tool being applied to mineralogical problems over the last two decades [2, 3 and references therein]. Coupled with more traditional "spot" analysis, more recent development of this technique as an imaging tool to map the distribution of trace element isotopes at the grain scale has helped validate models of ore formation at the deposit scale. The rapid and relatively inexpensive nature of the technique coupled with its excellent detection limits, complements other traditional elemental microanalysis techniques commonly used, such as scanning electron microscopy (SEM) and electron probe microanalysis (EPMA).

The combination of all these techniques – in situ on the same sample – allow for generation of large, representative datasets informing about elemental deportment in ore or gangue minerals that can aid in the development of models for ore genesis, underpin geochemical vectors for mineral exploration, and help guide optimisation of mineral processing strategies [3]. The LA-ICP-MS platform also offers the capability for rapid in-situ geochronology, providing important temporal constraints on ore-forming processes [4]. Commonly, U-Pb dating is applied to minerals such as zircon and monazite but is rapidly being extended to other dateable minerals more readily relatable to mineralising and alteration events, including hematite, apatite, cassiterite and epidote-group minerals.

3.1. Spot analysis versus elemental maps

Traditional LA-ICP-MS analysis consists of focussing a beam of pulsed UV light at a fixed position on the surface of a sample at which ablation will occur. The energy of the laser beam is transferred to the material and if above the ablation threshold volatilisation of the sample will occur. This volatilisation involves the formation of nanoparticles composed of the ablated material, which are transported via gas flow (usually He+Ar mix) from the ablation site into an ICP-MS where the elements of interest are measured. Many analytical aspects in both the laser and analysis mass spectrometer need to be considered for quality analyses, including, but certainly not limited to, factors such as downhole fractionation at the site of ablation (e.g., [5, 6]), mass bias within the spectrometer [7], standards used for quantitative analysis (e.g., [8]) and isobaric interferences.

The spatial resolution of analysis is inherently tied to the size of the laser beam used for analysis, and can be varied within each manufacturers software, usually anywhere from a few micrometre up to 100's of μm in diameter. However as elemental detection in ICP-MS is a physical transport process of ablated particles into a mass spectrometer, larger diameter laser spots give better detection limits due to the greater volume of ablated material and thus larger quantities of nanoparticles produced. As such typical quantitative laser ablation of minerals use spots sizes ranging from tens of microns to ~ 100 μm. As such, LA-ICP-MS will never approach the spatial resolution offered by e-beam techniques such as EPMA, however it provides superior detection limits for multiple isotopes of a single element, usually in the ppb-range, at least for most heavy elements, with elements traditionally difficult to measure such as REE (due to interference issues) becoming relatively straightforward in a variety of matrices such as feldspars [9], apatite [10], or hematite [11, 12].

During spot analysis, traditionally the laser beam is kept firing at a single location for on average ~ 0.5 - 1 minute depending on the purpose of analysis. During this period, we are measuring the isotopes of elements of interest repeatedly to give us time-resolved analysis. Due to the nature of laser ablation, we are continuously drilling down into our mineral of interest, and as such the time-resolved signal acquired relates to how each of the measured masses are changing subsurface. The depth of the ablation pit over the course of each analysis is highly dependent on the laser energy utilised and nature of the mineral matrix being ablated and can range anywhere from a few μm to tens of μm deep in the case of soft sulphides like galena or chalcopyrite [13]. Figure 1 displays some typical downhole spot analysis profiles from the mineral hematite (α-Fe_2O_3). The elemental trends downhole reflects a combination of the homogeneity of the mineral being ablated (i.e., does the mineral contain any inherent chemical zonation?), in addition to the presence of other minerals as micro-/nanoscale inclusions within the primary mineral (seen as "spikes" in certain elements, at least in case when those inclusions are of sufficient size).

This measurement volume differs to normal e-beam methods of measurement such as EPMA, where at operating conditions of 15 kV interaction volumes in hematite are on the order of one micrometre (ignoring secondary fluorescence effects).

The more recent development of utilising LA-ICP-MS as a trace element mapping tool has allowed visualisation of elemental distributions that would require extreme analytical conditions, or otherwise impossible to detect via traditional e-beam methods. The process involves setting up a series of parallel laser rasters over the area of interest, along which the laser beam travels at a speed set by the user. In this way time resolved intensity data is collected, which can be stitched together into a 2D images with commercial software and quantified if the appropriate microanalytical standards are available. Figure 2 displays an example of LA-ICP-MS maps of an aggregate of pyrite grains.

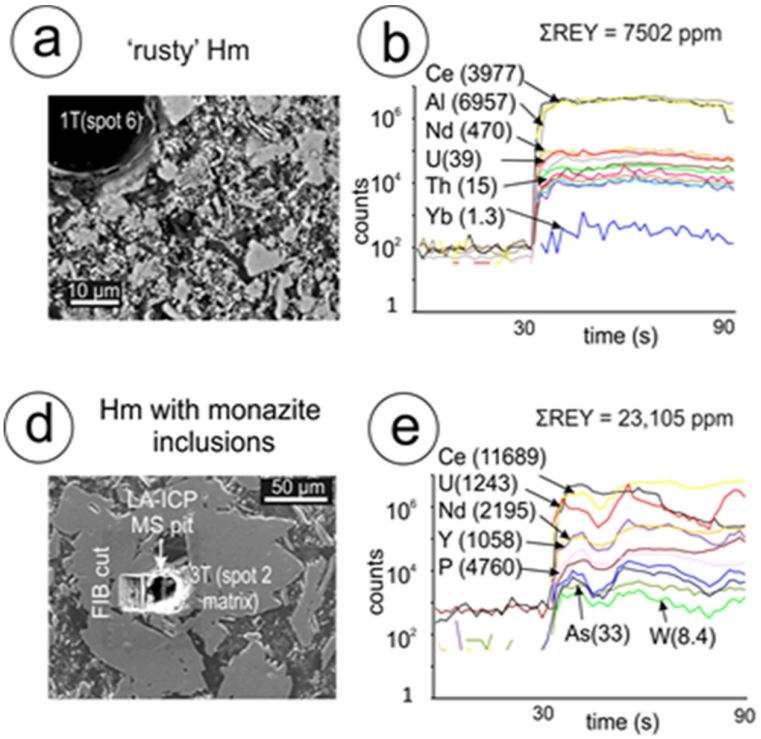

Figure 1. a) and d) Secondary electron (SE) images of hematite from Olympic Dam, South Australia; b) Time-resolved downhole elemental intensities of laser pit shown in (a). Note consistent flat elemental profiles indicating either homogeneous material is being ablated or that these elements occur as evenly distributed nanoscale inclusions within hematite; e) Time resolved downhole profile of laser pit shown in (d). Note uneven nature of signals for P and REE, suggesting the presence of subsurface micrometre-sized monazite inclusions. FIB-SEM extraction of a foil taken adjacent to ablation pit, and subsequent analysis by TEM confirmed the presence of monazite inclusions. Figure reproduced from [3].

Immediately obvious in Fig. 2 is the oscillatory zoning in As, Co, and Ni, which represent minor element concentrations (1000's of ppm) that would otherwise be measurable by X-ray mapping techniques such as EPMA, albeit at a worse signal/noise ratio. These three elements occur within solid solution in pyrite, often displaying oscillatory zoning patterns. The remaining mapped elements illustrated (Ga, Ag, Bi, and W) are present in much lower concentrations (maximum of a few hundred ppm), and display a drastically different elemental distribution. Silver and bismuth in particular display elevated concentrations of these elements along both fractures and cleavage planes within the pyrite grains, the latter usually invisible in typical back-scattered electron (BSE) SEM imaging. The concentration levels of these elements would make them undetectable by normal e-beam techniques. LA-ICP-MS mapping allows heterogeneous distributions of trace elements present at concentrations of just a few ppm to be seen clearly (e.g., the fine-scale Te- and Se-zoning in arsenopyrite [14]).

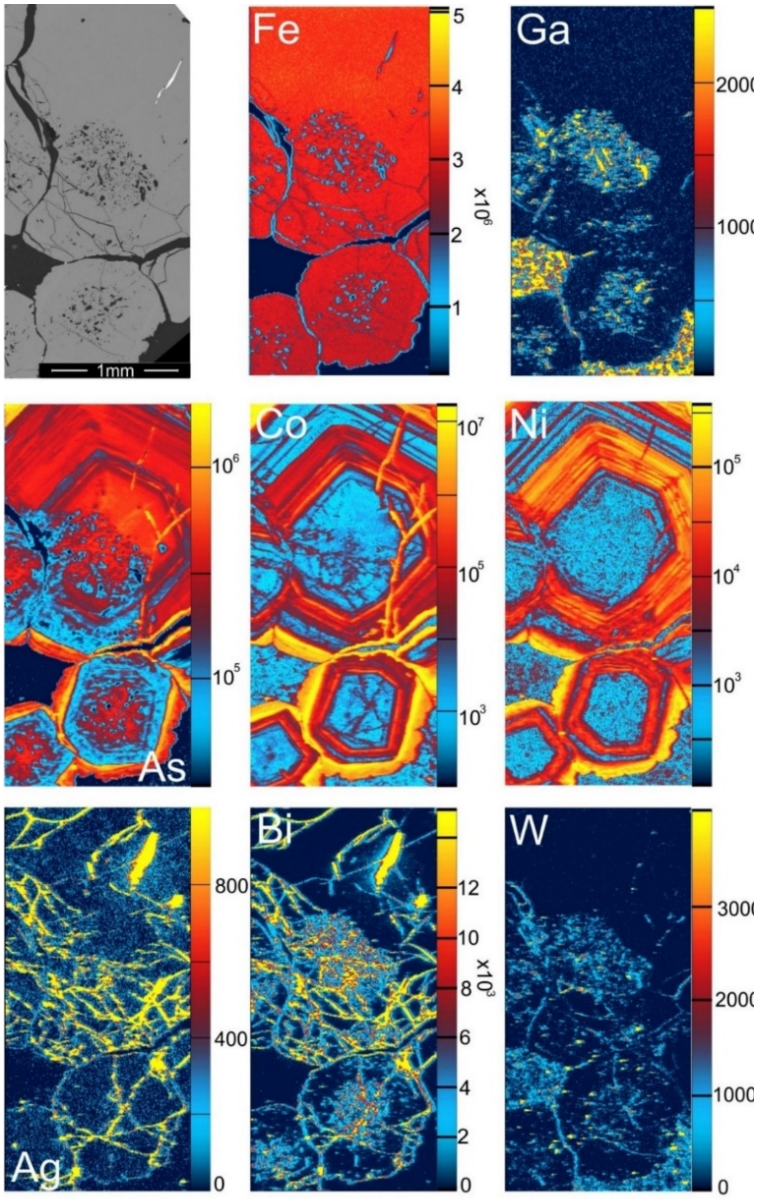

Figure 2. Laser ablation maps of pyrite grains. Intensity colour scale in CPS. Note oscillatory zoning of As, Co, and Ni, indicating solid solution lattice bound elements within pyrite. Ga, Ag, Bi, W display elevated concentration along microfractures and cleavage planes. The mapped area is shown as a backscatter electron image at upper left. Scales in counts-per-second. Measured isotopes: ^{56}Fe, ^{69}Ga, ^{75}As, ^{59}Co, ^{60}Ni, ^{109}Ag, ^{209}Bi, ^{182}W. Figure reproduced from [3].

LA-ICP-MS mapping removes the inherently biased nature of the alternate option of a spot traverse over the mineral in question, and often reveals elemental distributions that would have otherwise been missed. Experience with different mineral matrices, including those for which only limited trace element data was hitherto available, e.g., baryte [15], indicates that a majority of minerals are chemically zoned, and thus spot analysis alone will not provide adequate

characterisation of trace element concentrations. The sensitive nature of the LA-ICP-MS mapping technique makes it very powerful when used in combination with other e-beam mapping techniques such as EPMA, or if complemented by other methods affording visualisation of distribution patterns at sub-micron (e.g., nanoSIMS) or nm-scale (e.g., TEM-EDS element mapping).

LA-ICP-MS mapping has two additional advantages over conventional spot analysis: Firstly, it allows a direct visualisation of the systematic preferential partitioning of trace elements between co-existing mineral phases, e.g., co-existing base metal sulphides [16] or common Cu-Pb-Sb-sulphosalts [17]. Secondly, the method allows for ready recognition of non-traditional mineral hosts for elements of interest (e.g., the occurrence of significant concentrations of U, Sn, Mo, and W within skarn garnet [18]).

3.2. New geochronological tools: microanalysis and standard development

Accurate determination of the timing of a mineralisation event can be challenging. This is often primarily due to the ambiguity of linking growth of the dated (gangue) mineral with the associated minerals hosting the metals of interest. In addition, these complex ore mineral systems may involve multiple phases of mineral growth and fluid flow events that can overprint textures and reset geochronological clocks, making unequivocal interpretation difficult. Whenever possible, it is desirable to directly date the ore minerals themselves – and successful attempts with minerals such as molybdenite, cassiterite, columbite-tantalite, and uraninite are well reported in the literature. Often, however, these datable minerals are absent or only found in very specific mineral deposits, and as such the geologist is usually bound to analysis of more traditional U-Pb geochronometers such as zircon, monazite, and rutile. However, the accessory refractory nature of these minerals and their propensity for age "inheritance" can make it difficult to directly relate the calculated age of these minerals to a mineralising event.

As such, effort has been made to identify potential new U-Pb mineral geochronometers. Hematite, a common Fe-oxide in many types of ore deposits, and the most abundant minerals in many iron oxide copper gold (IOCG) deposits. The presence of U- and Pb-bearing hematite at Olympic Dam [19], the world's largest IOCG-type deposit [20], therefore, raised the question of whether the mineral could be accurately and precisely dated. Textural evidence for crystallisation of hematite at the same time as Cu mineralisation allows age relationships to established with confidence. The high levels, and grain-scale distribution of U endowment in Olympic Dam hematite were first quantified by Ciobanu *et al.* [21]; additional data and LA-ICP-MS maps are given by Verdugo-Ihl *et al.* [11]. These studies showed that hematite readily accepts up to wt% levels U and radiogenic Pb into its crystal structure without major structural modification or radiogenic damage to its lattice due to α-decay (Figs. 3 and 4).

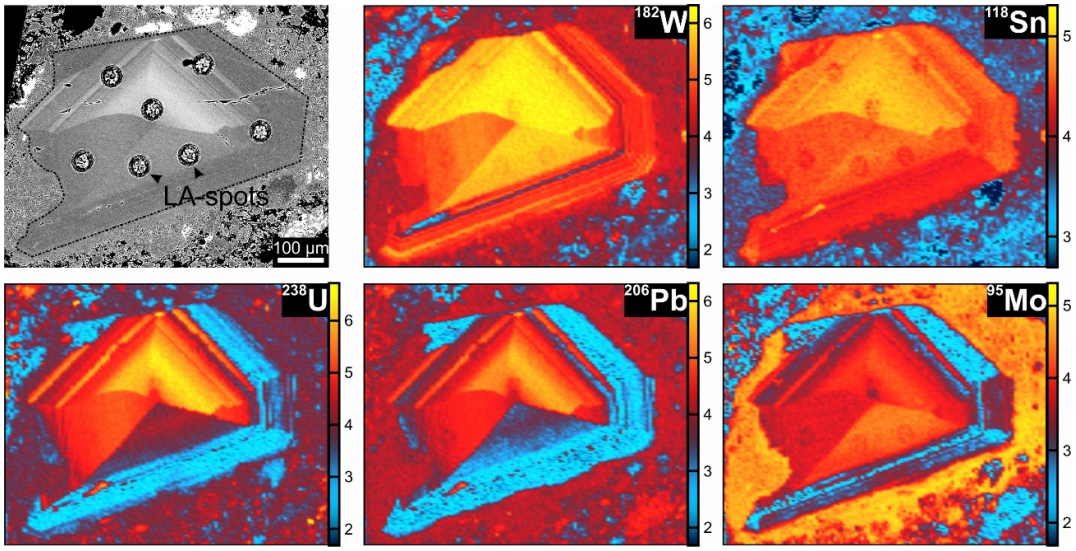

Figure 3. Laser ablation elemental maps of hematite grains. Note elevated levels of U and Pb in the oscillatory-zoned core domain (up to 1000 ppm), and 100's to 1000's ppm of W, Sn, and Mo. Scales in cps (x 10n). Figure adapted from [11].

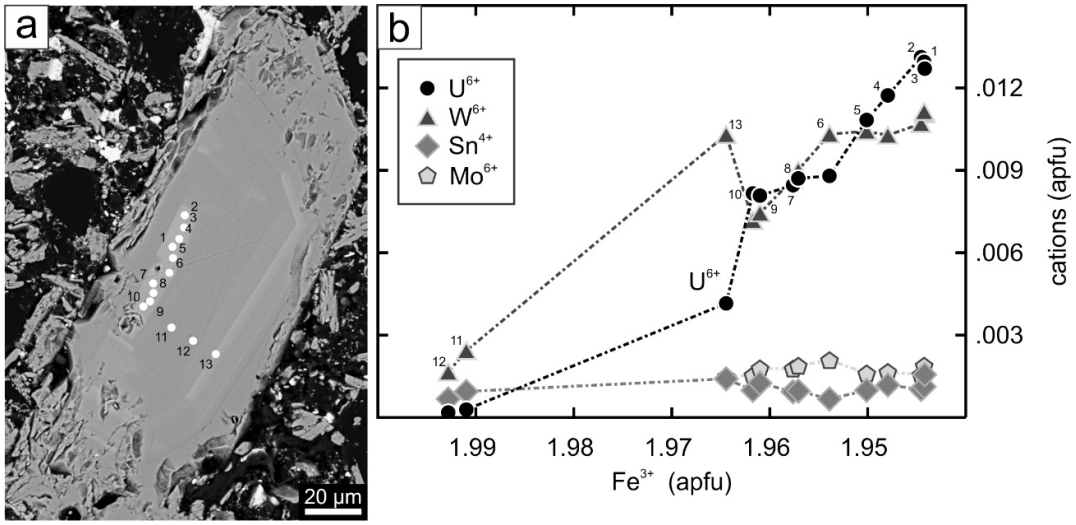

Figure 4. a) BSE image of a typical hematite grain displaying zonation as bright zones. Spots represent EPMA analytical locations. b) EPMA compositional spot data of grain displayed in (a). Note increasingly elevated U and W values corresponding with bright zones in BSE. Figure adapted from [11].

Ciobanu *et al.* [21] attempted to date these grains via LA-ICP-MS and since then, additional efforts have been made to date Olympic Dam hematite with similar results [22, 23]. Courtney-Davies *et al.* [22] also provided U-Pb hematite age for mineralization from Carajas, Brazil. Recently, Keyser *et al.* [24] gave a U-Pb hematite age for upgrading of banded iron formation iron ores from the Middleback Ranges, South Australia, using hematite that contained just 7 - 24 ppm U. This demonstrates both the versatility and huge potential of the new method.

In the absence of U-Pb hematite reference material, both studies utilised a zircon reference material to correct U-Pb data. As discussed in previous sections, the process of laser ablation is a physical process in which the sample is volatilised, and ablated material is transported to the ICP-MS as nanoparticles. As such, different minerals ablate differently dependant on their composition, resulting in a different downhole U-Pb ratio profile between hematite and zircon. This results in inaccuracies in determination of U-Pb ratios of hematite when using zircon as a standard.

To circumvent this problem, suitable samples have been sent for U-Pb analysis via "standardless" isotope dilution thermal ionisation mass spectrometry (ID-TIMS) and begun development of a synthetic hematite U-Pb microanalytical standard. Initial ID-TIMS results give excellent accuracy and precision with expected age of the mineralisation event (Fig. 5; [23]). Although accepted as the "gold standard" of U-Pb analysis, ID-TIMS is a time-consuming and costly process and a need was recognised for more routine fast U-Pb analysis of hematite grains via microbeam techniques such as LA-ICP-MS or SHRIMP. To achieve this hydrated ferric oxide (HFO) has been doped with a U and Pb solution, homogenised, dried, and then converted to hematite via heating to ~ 700 °C (Fig. 6; [25]). The resultant hematite chips display encouraging homogeneity in U-Pb ratio and concentration and are currently being further refined and analysed via ID-TIMS for certification.

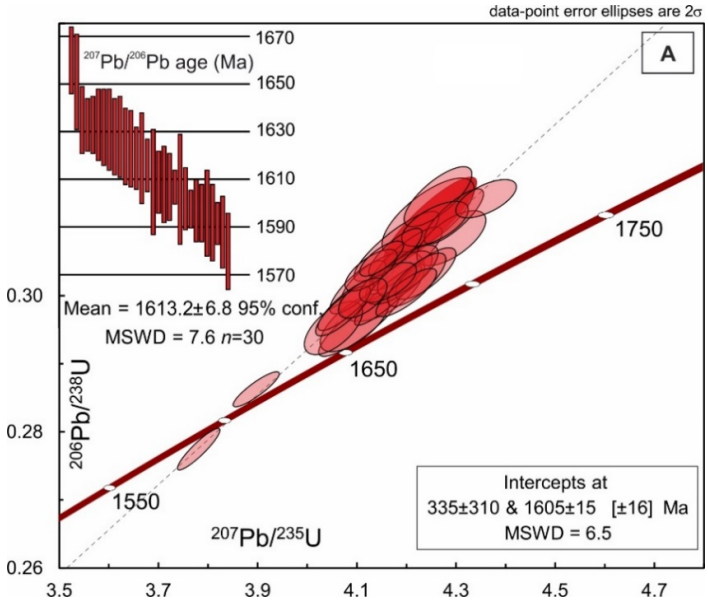

Figure 5. U-Pb concordia diagram adapted from Courtney-Davies *et al.* [23] displaying weighted mean and intercept ages of ~ 1,600 Ma. Note "reverse discordance" of data ellipses sitting above concordia line. This is predominantly an analytical artefact induced by correcting U-Pb ratios in analysed hematite against a zircon reference material.

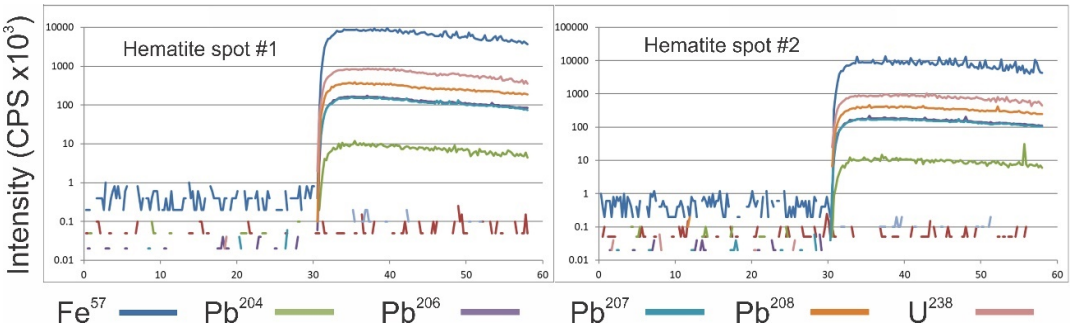

Figure 6. Representative time-resolved analysis of two separate chips. Note inhomogeneous downhole signal ^{204}Pb in spot #2, indicating some subsurface heterogeneity. Figure adapted from [25].

4. HIGH-RESOLUTION TRANSMISSION ELECTRON MICROSCOPY

The range of techniques discussed here represent a broad spectrum in spatial resolution, ranging from exceptional elemental detection limits at scales of several to a few tens of micrometres, to higher resolution imaging and elemental analysis of features on polished block surfaces that may only be a few nanometres in size. Transmission electron microscopy (TEM) extends this range substantially, enabling imaging and powerful analytical techniques ranging from the micrometre-scale down to the scale of individual atoms.

4.1. Sample preparation - Focussed ion beam milling

Samples for TEM analysis must be thinned to electron transparency, well below 200 nm, ideally ~ 60 nm. An important aspect of using a multiplatform approach is the ability to link regions of interest between techniques, which can make the precise extraction of a suitable TEM sample challenging. In order to study a specific feature within a mineral using TEM (such as a grain boundary, or compositionally-zoned domain within a specific grain), a precise method is required to extract an extremely thin section at the required location. This section must also be extracted at an exact orientation, in order to ultimately visualise the crystal lattice at the desired orientation, allowing the observation of specific grain boundaries and defects. This process is shown in Fig. 7.

Dual-beam instruments have proven invaluable for in-situ preparation of TEM samples in a range of fields, including materials science, metallurgy, earth science and the semiconductor industry. These focussed ion beam – scanning electron microscopes (FIB-SEM) incorporate a traditional SEM column for non-destructive imaging, and an ion column utilising heavy ions (e.g., Ga, Xe, Ar) for imaging and precise milling of the sample. The imaging/milling capability allows regions in a mineral to be precisely identified, which can be of significant advantage when that mineral has been comprehensively characterised prior to FIB-SEM work (by SEM, EPMA and

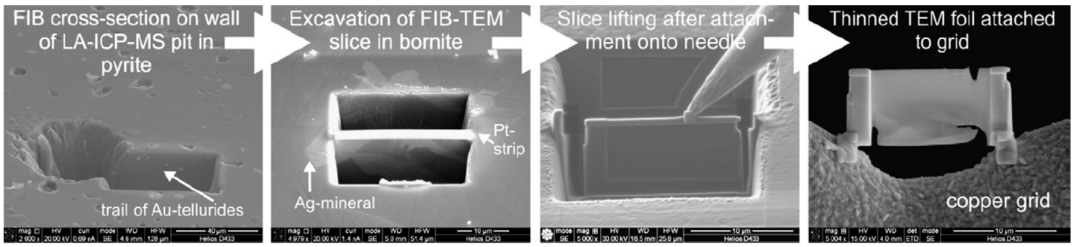

Figure 7. Sequence of analytical procedures for FIB–TEM foil preparation. Figure adapted from [26].

LA-ICP-MS). A thin TEM cross-section (or foil), is milled and lifted from the sample. A range of artefacts that can result from milling and thinning of ore mineral, e.g. via interaction with the Ga+ source, melting, etc., have been highlighted in Ciobanu *et al.* [26].

4.2. Scanning transmission electron microscopy

Scanning transmission electron microscopy (STEM), in particular high angle annular dark-field (HAADF STEM) is proving to be an exceptional technique for the characterisation of minerals from ores. In STEM mode, the incident electron beam is focussed into a small probe and raster-scanned across the sample surface, in a similar manner to the SEM. The difference between these techniques lies in the transmission of the beam through the sample, where post-sample detectors collect the electrons from different interaction events with the specimen. Although many signals are accessible simultaneously, of particular relevance is the HAADF detector. This detector is an annular type, which allows electrons with little or no scattering to pass through, while collecting the electrons scattered at high angles due to strong interactions with the atomic nuclei. The HAADF signal, importantly, is incoherent and monotonic, scaling with the thickness of the sample by $I = t$ and the elemental mass by $I = Z^{\sim 2}$.

The Z-contrast observed by HAADF STEM positions the technique as exceptional for characterising minerals of direct relevance to ore deposit studies, allowing the rapid identification of fine particles (100 - 2,500 nm) and ultrafine nanoparticles (1 - 100 nm) as inclusions, layer stacking in mixed layer compounds, crystal-structural motifs in large structures such as Pb-Bi-sulphosalts, as well as atom-scale defects. In addition to this, the incoherent nature of the signal results in atomic resolution images, which are readily interpretable, showing the location of atoms in the lattice directly and, in simple cases, suggesting the atomic species based on observed Z contrast. Experience has shown that HAADF STEM imaging is particularly well-suited to modular minerals composed of atomic layers that differ markedly in composition and thus contrast on the images.

The ability to directly visualise these crystal structures is valuable for several reasons. Firstly, modular minerals (notably Pb-Bi-sulphosalts) may belong to structurally-defined homologous series in which changes in chemistry are accommodated by incremental changes in homology [27, 28]. Secondly, there may exist multiple polytypes, and potentially, new mineral species,

that occupy compositional space between end-members, and which can be built by combinations of two or more building blocks. For example, there exist at least 11 distinct polytypes in the bastnäsite-synchysite group of rare earth element fluorocarbonates that can be directly imaged in terms of combinations of bastnäsite (B) and synchysite (S) layers, B2S, BS, BS2 etc. (Fig. 8; [29]). Thirdly, layered minerals commonly display non-stoichiometry at the scale of the electron microprobe, a phenomenon readily explained by irregular, or semi-regular intergrowths (of various amplitude) of layers at the lattice scale, as for example in Bi-chalcogenides of the tetradymite group [30] – minerals commonly found in gold deposits (e.g., [31]) and the natural equivalents of some of the best semi-conductors known. The capabilities of HAADF STEM imaging are clearly observed for the mineral tellurobismuthite, Bi_2Te_3, which displays distinct Z-contrast for the bismuth and tellurium atoms as shown in Fig. 9.

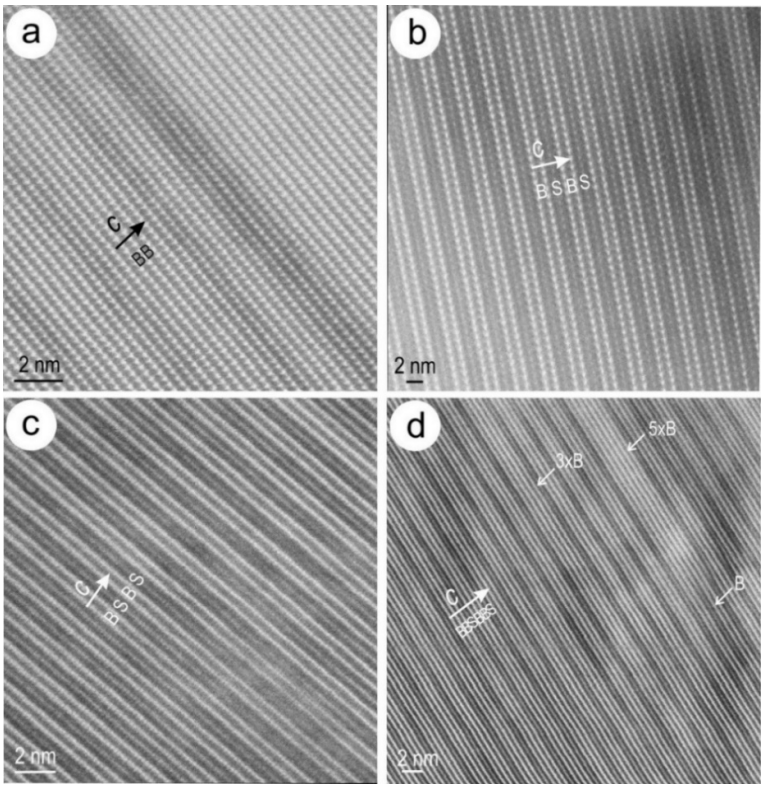

Figure 8. HAADF STEM images showing a) the typical stacking sequences in bastnäsite down to [−1100]; b and c) Parisite down to [−1100] and [10–10] zone axis, respectively. The sequence is characterised by two rows of bright atoms (B slab) and one row of slightly darker atoms ('f' layer in the middle of the S slab); and d) B_2S imaged down to [10–10] zone axis. Figure reproduced from [29].

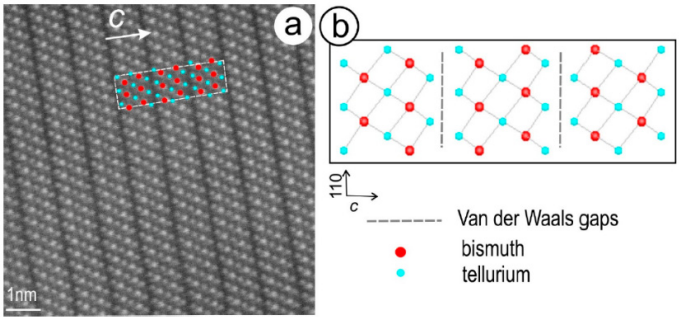

Figure 9. a) High-resolution HAADF STEM image of tellurobismuthite (Bi_2Te_3), and b) Crystal structure model for the mineral, showing the positions of the atoms and the Van der Waals gaps between the layers. Figure reproduced from [1].

4.3. Incorporation and release of trace elements in ore minerals

The high resolution and Z contrast achievable by HAADF STEM make the technique ideal for study of lattice-scale incorporation and release of heavy elements into and from mineral matrices. One good example is uranium within the crystal lattice of hematite. Studies of U-being hematite are important for development of U-Pb geochronology, as documented above, and also for mineral processing. In U-W-Sn-Mo oscillatory-zoned hematite from Olympic Dam that experienced overprinting [11], uraninite nanoparticles were identified (Fig. 10) from domains where fluid percolation assisted U release from the crystal lattice of hematite and led to crystal zoning re-shaping.

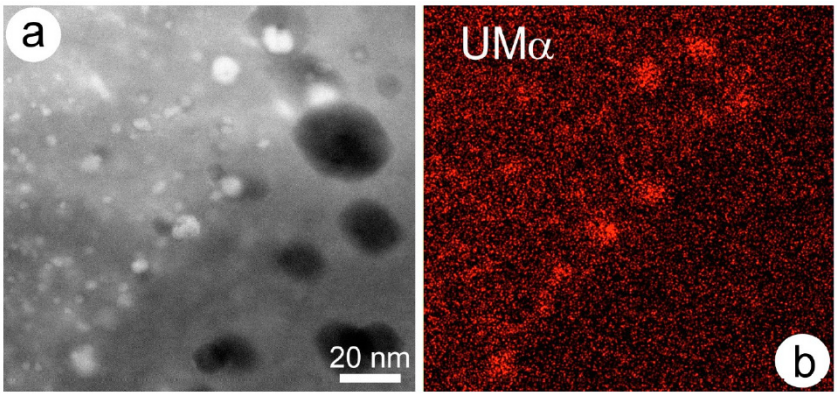

Figure 10. Hematite mineral from the Olympic Dam orebody, showing a) HAADF STEM image of uraninite nanoparticles, and b) EDS map of the imaged area, confirming the distribution of uranium. Figure reproduced from [1].

HAADF STEM study of FIB-prepared foils extracted from across zoning in hematite containing some of the most U (up to 2 - 3 wt% UO_2) from Olympic Dam shows instead presence U-free

nanometre-scale needles of magnetite (Fe_3O_4) [32]; Fig. 11). Lattice scale faults assist transformation of the rhombohedral hematite [1-10] into the cubic magnetite [1-10] lattice (Fig. 11a). The epitaxial relationships between the two Fe-oxides are preserved in the widest needles (10 – 20 nm wide; Fig. 11b). Identification of magnetite against other phases such as cubic (β-, or γ-) Fe_2O_3 polymorphs is based upon EDS-STEM mapping showing higher-Fe and lower-O composition of the needle relative to host hematite as well, as by STEM simulation of the images (Fig. 11c). Such needles are not found in domains of high-W (up to several wt% WO_3) or low-U (up to thousands of ppm U) hematite. Results suggest that such magnetite needles only occur at the upper U solubility limit in the U-bearing hematite lattice. This is most significant for understanding reliability of such grains for high-precision U-Pb dating.

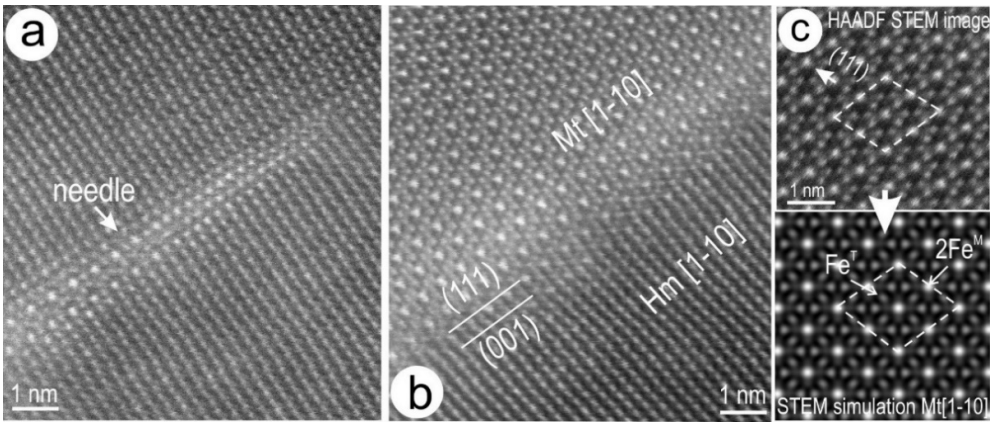

Figure 11. HAADF STEM images showing needles of magnetite (Mt) in U-rich hematite (Hm): A few atoms in width a) and some tens of nm-wide b). c) Image and STEM simulation of Mt on [1-10] zone axis. T = tetrahedral site; M = octahedral site. Images obtained at 200 kV. STEM simulation using WinHREMTM version 4.1 software. Figure adapted from [32].

4.4. Other crystal structural modifications: superstructures

Phase transitions and crystal structural modifications can occur in mineral that crystallise from high temperature solid-solutions; Cu-Fe-sulphides are a typical example. Cu-Fe-sulphides from different ore zones at Olympic Dam feature nanoscale intergrowths, superstructure domains (larger structures built from a simpler crystal structure in which mixed sites, vacancies, or impurities are ordered over 'n' unit cells) and antiphase boundary domains that can be interpreted as exsolution, coarsening and phase transformation during cooling from high-T solid solutions in the system Cu-Fe-S and sub-systems according to published phase diagrams [34]. Bornite (Cu_5FeS_4) superstructures are formed by Fe vacancy ordering [35]. These (Fig. 12) are documented for the first time by HAADF STEM imaging of Cu-ores from South Australia [33].

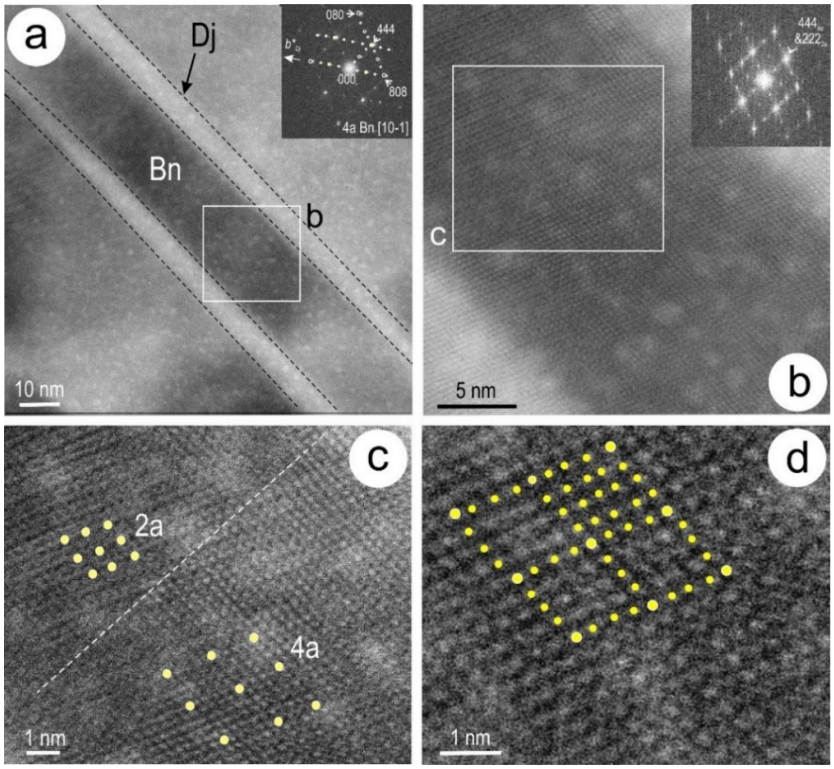

Figure 12. Atomic-scale HAADF STEM images of bornite superstructures down to the [101] zone axis. a) Bornite with marginal djurleite. FFT (inset) shows coherent intergrowths between 4a bornite and djurleite. b) Close-up of the area marked in (a) showing domain heterogeneity throughout the bornite. Satellite reflections (FFT in inset) shows four-fold periodicity but with variation in intensity indicating the co-existence of 2a and 4a superstructures. c) 2a and 4a superstructure domains in the area marked in (b). Yellow dots highlight structural motifs for the two species. d) Detail of 4a superstructure showing atom distribution throughout the superlattice as marked by the yellow dots. Note faint variation in grey-scale intensity of the atoms that make the superstructure unit cell. Bn = bornite; Dj = djurleite. Figure adapted from [33].

5. CONCLUDING REMARKS

Using different techniques on the same sample material, bridging scales of observation from that of mm down to Ångstroms, and proceeding from least- to most-destructive, has facilitated significant advances in the research field. In particular, samples extracted in-situ by FIB-SEM after micrometre-scale characterisation possess extraordinary versatility. Not only can HAADF STEM imaging provide insights down to the nanoscale but FIB-prepared foils can be readily examined by electron backscatter diffraction (EBSD) to understand crystal orientations and modification thereof (as applied to uraninite; [36]), or synchrotron X-ray studies to determine the speciation of component ions (as applied to Cu in sphalerite; [37]).

6. ACKNOWLEGEMENTS

Much of the research reported here was funded from the ARC Research Hub for Australian Copper-Uranium (Grant IH130200033) and the 'FOX' project, supported by BHP Olympic Dam and the South Australian Government Mining and Petroleum Services Centre of Excellence.

7. REFERENCES

[1] Cook N J, Ciobanu C L, Ehrig K, Slattery A, Verdugo-Ihl M R, Courtney-Davies L and Gao W 2017 Advances and opportunities in ore mineralogy. *Minerals* **7** 233

[2] Sylvester P (Ed.) 2008 Laser ablation ICP□MS in the Earth Sciences: Current practices and outstanding issues. *Mineral. Ass. Canada* **40** (Québec, QC, Canada)

[3] Cook N J, Ciobanu C L, George L and Ehrig K 2016 Trace element analysis of minerals in magmatic-hydrothermal ores by laser ablation inductively-coupled plasma mass spectrometry: Approaches and opportunities. *Minerals* **6** 111

[4] Woodhead J D, Horstwood M S A and Cottle J M 2016 Advances in isotope ratio determination by LA-ICP-MS. *Elements* **12** 317-322

[5] Gilbert S E, Danyushevsky L V, Goemann K and Death D 2014 Fractionation of sulphur relative to iron during laser ablation□ICP□MS analyses of sulphide minerals: Implications for quantification. *J. Anal. Atom. Spectrom.* **29** 1024-1033

[6] Zhu Z Y, Jiang S Y, Yang T, Ciobanu C L and Cook N J 2016 Sulfur isotope fractionation in pyrite during laser ablation: Implications for laser ablation multiple collector inductively coupled plasma mass spectrometry mapping. *Chem. Geol.* **450** 223-234

[7] Günther D and Koch J 2008 Formation of aerosols generated by laser ablation and their impact on elemental fractionation in LA□ICP□MS. in: Laser ablation ICP□MS in the Earth Sciences: Current practices and outstanding issues (P. Sylvester; Ed.) *Mineral. Ass. Canada* **40** 19-34 (Québec, QC, Canada)

[8] Danyushevsky L, Robinson P, Gilbert S, Norman M, Large R, McGoldrick P and Shelley M 2011 Routine quantitative multi□element analysis of sulphide minerals by laser ablation ICP□MS: Standard development and consideration of matrix effects. *Geochem. Explor. Environ. Anal.* **11** 51-60

[9] Kontonikas-Charos A, Ciobanu C L, Cook N J, Ehrig K, Krneta S and Kamenetsky V S 2017 Feldspar evolution in the Roxby Downs Granite, host to Fe-oxide Cu-Au-(U) mineralisation at Olympic Dam, South Australia. *Ore Geol. Rev.* **80** 838-859

[10] Krneta S, Ciobanu C L, Cook N J, Ehrig K and Kontonikas-Charos A 2017 Rare earth element behaviour in apatite from the Olympic Dam Cu-U-Au-Ag deposit, South Australia. *Minerals* **7** 135

[11] Verdugo-Ihl M R, Ciobanu C L, Cook N J, Ehrig K J, Courtney-Davies L and Gilbert S 2017 Textures and U-W-Sn-Mo signatures in hematite from the Olympic Dam Cu- U-Au-Ag deposit, South Australia: Defining the archetype for IOCG deposits. *Ore Geol. Rev.* **91** 173-195

[12] Keyser W M, Ciobanu C L, Cook N J, Johnson G , Feltus F, Johnson S, Dmitrijeva M, Ehrig K and Nguyen P 2018 Petrography and trace element signatures of iron-oxides in deposits from the Middleback Ranges, South Australia: from banded iron formation to ore. *Ore Geol. Rev.* **93** 337-360

[13] George L, Cook N J, Ciobanu C L and Wade B P 2015 Trace and minor elements in galena: A reconnaissance LA-ICP-MS study. *Amer. Mineralogist* **100** 548-569

[14] Cook N J, Ciobanu C L, Meria D, Silcock D and Wade B 2013 Arsenopyrite-pyrite association in an orogenic gold ore: tracing mineralization history from textures and trace elements. *Econ. Geol.* **108** 1273-1283

[15] Schmandt D S, Cook N J, Ehrig K, Gilbert S, Wade B P, Rollog M, Ciobanu C L and Kamenetsky V S 2019 Uptake of trace elements by baryte during copper ore processing: A case study from Olympic Dam, South Australia. *Minerals Engng.* **135** 83-94

[16] George L L, Cook N J and Ciobanu C L 2016 Partitioning of trace elements in co-crystallized sphalerite-galena–chalcopyrite hydrothermal ores. *Ore Geol. Rev.* **77** 97-116

[17] Li W, Cook N J, Ciobanu C L, Xie G Q, Wade B P and Gilbert S E 2019 Trace element distributions in (Cu)-Pb-Sb sulfosalts from the Gutaishan Au-Sb deposit, South China: Implications for formation of high fineness native gold. *Amer. Mineralogist* **104** 425-437

[18] Xu J, Ciobanu C L, Cook N J, Zheng Y, Sun X and Wade B P 2016 Skarn formation and trace elements in garnet and associated minerals from Zhibula copper deposit, Gangdese Belt, southern Tibet. *Lithos* **262** 213-231

[19] Oreskes N 1990 Uranium content of Olympic Dam hematite: Implications for fluid chemistry and ore depositional mechanisms. in: *Program with Abstracts of the 8th Quadrennial IAGOD Conference*. (Ottawa, Canada) A137

[20] Ehrig K, McPhie J and Kamenetsky V 2012 Geology and mineralogical zonation of the Olympic Dam iron oxide Cu-U-Au-Ag deposit, South Australia. in: Geology and genesis of major copper deposits and districts of the World: A tribute to Richard H. Sillitoe. (Hedenquist J W, Harris M and Camus F; Eds.). *Soc. Econ. Geol.* **Spec. Publ. 16** 237-267

[21] Ciobanu C L, Wade B, Cook N J, Schmidt Mumm A and Giles D 2013 Uranium-bearing hematite from the Olympic Dam Cu-U-Au deposit, South Australia; a geochemical tracer and reconnaissance Pb-Pb geochronometer. *Precambr. Res.* **238** 129-147

[22] Courtney-Davies L, Zhu Z, Ciobanu C L, Wade B P, Cook N J, Ehrig K, Cabral A R and Kennedy A 2016 Matrix-matched iron-oxide laser ablation ICP-MS U-Pb geochronology using mixed solution standards. *Minerals* **6** 85

[23] Courtney-Davies L, Tapster S R, Ciobanu C L, Cook N J, Verdugo-Ihl M R, Ehrig K J, Kennedy A K, Gilbert S E, Condon D J and Wade B P 2019 A multi-technique evaluation of hydrothermal hematite U-Pb isotope systematics: Implications for ore deposit geochronology. *Chem. Geol.* **513** 54-72

[24] Keyser W, Ciobanu C L, Cook N J, Dmitrijeva M, Courtney-Davies L, Feltus H, Gilbert S, Johnson G and Ehrig K 2019 Iron-oxides constrain BIF evolution in terranes with protracted geological histories: The Iron Count prospect, Middleback Ranges, South Australia. *Lithos* **324** 20-38

[25] Courtney-Davies L, Ciobanu C L, Richardson M W, Prosser N, Verdugo-Ihl M, Wade B P, Gilbert S E, Ehrig K J and Cook N J 2019 Synthesis of U-Pb doped hematite using a hydrated ferric oxide approach. *J. Crystal Growth* **513** 48-57

[26] Ciobanu C L, Cook N J, Utsunomiya S, Pring A and Green L 2011 Focussed ion beam - transmission electron microscopy applications in ore mineralogy: bridging micron- and nanoscale observations. *Ore Geol. Rev.* **42** 6-31

[27] Ciobanu C L, Cook N J, Maunders C, Wade B P and Ehrig K 2016 Focused ion beam and advanced electron microscopy for minerals: Insights and outlook from bismuth sulphosalts. *Minerals* **6** 112

[28] Li W, Ciobanu C L, Slattery A, Cook N J, Liu W, Wade B P and Xie G Q 2019 Chessboard structures: atom-scale imaging of homologues from the kobellite series. *Amer. Mineralogist* **104** 459-462

[29] Ciobanu C L, Kontonikas-Charos A, Slattery A, Cook N J, Ehrig K and Wade B P 2017 Short-range stacking disorder in mixed-layer compounds: A HAADF STEM study of bastnäsite-parisite intergrowths. *Minerals* **7** 227

[30] Ciobanu C L, Pring A, Cook N J, Self P, Jefferson D, Dima G and Melnikov V 2009 Chemical-structural modularity in the tetradymite group: a HRTEM study. *Amer. Mineralogist* **94** 517-534

[31] Ciobanu C L, Birch W D, Cook N J, Pring A and Grundler P V 2010 Petrogenetic significance of Au-Bi-Te-S associations: the example of Maldon, Central Victorian gold province, Australia. *Lithos* **116** 1-17

[32] Ciobanu C L, Slattery A, Verdugo-Ihl M, Courtney-Davies L, Cook N J and Ehrig K 2018 Crystal structural modifications in U-rich, oscillatory-zoned hematite. in: *Abstracts of Goldschmidt-2018*. (Boston, MA, USA; 12-17 August)

[33] Owen N D, Ciobanu C L, Cook N J, Slattery A and Basak A 2018 Nanoscale study of clausthalite-bearing symplectites in Cu-Au-(U) ores: Implications for ore genesis. *Minerals* **8** 67

[34] Ciobanu C L, Cook N J and Ehrig K 2017 Ore minerals down to the nanoscale: Cu-(Fe)-sulphides from the iron oxide copper gold deposit at Olympic Dam, South Australia. *Ore Geol. Rev.* **81** 1218-1235

[35] Ding Y, Veblen D R and Prewitt C T 2005 High-resolution transmission electron microscopy (HRTEM) study of 4a and 6a superstructure of bornite Cu5FeS4. *Amer. Mineralogist* **90** 1256-1264

[36] Macmillan E, Ciobanu C L, Ehrig K, Cook N J and Pring A 2016 Replacement of uraninite by bornite via coupled dissolution-reprecipitation: Evidence from texture and microstructure. *Can. Mineralogist* **54** 1369-1383

[37] Cook N J, Etschmann B, Ciobanu C L, Howard D, Williams T, Rae N, Pring A, Geraki K, Chen G R and Brugger J 2015 Synchrotron XANES study of a Ge-(Fe)-bearing sphalerite. *Minerals* **5** 117-132